THE JOURNAL OF PHYSICAL CHEMISTRY B

ARTICLE

pubs.acs.org/JPCB

Sorption on Deformable Solids. Density Functional Theory Approach

Gersh O. Berim and Eli Ruckenstein*

Department of Chemical and Biological Engineering, State University of New York at Buffalo, Buffalo, New York 14260, United States

ABSTRACT: A modified density functional theory is proposed to describe fluid adsorption and absorption by a solid, the density of which is nonhomogeneous near the interface. The density distribution of the solid is not provided by apriori assumptions, but is obtained via the minimization of an appropriate thermodynamic potential. The theory considers a mixture of two components in a slitlike pore. One of them, the fluid, is in contact with a reservoir containing the same kind of molecules and can be described through a grand canonical ensemble. The other component has strong interactions between its molecules. As a consequence, it forms a solid in the slit which can be treated as a canonical ensemble of a fixed number of molecules. The theory predicts both an intrinsic (in the absence of fluid) change in the solid density near the interface and a solid density variation as the fluid density in the reservoir is changed. In addition, it reveals that the oscillations that occur in the fluid density when the solid density is uniform are damped by the nonuniform solid. The theory provides the amounts of fluid adsorbed as well as absorbed by the solid.

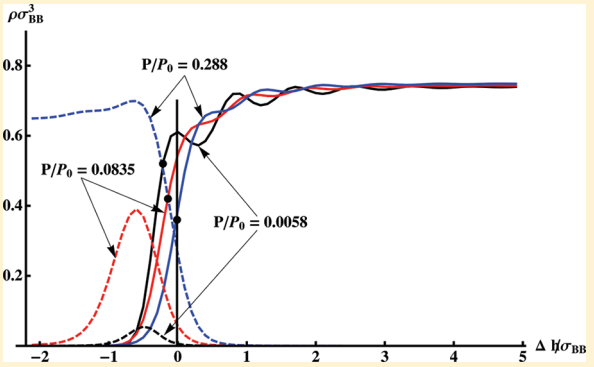

1. INTRODUCTION

Most existing microscopic theories describing a fluid in contact with a solid (such as, for instance, the density functional theory) treat the solid as a continuous uniform body. This implies that there is a well-defined surface of the solid at which its density drops down to zero in a discontinuous manner. The interactions between the solid and fluid molecules are usually described by a Lennard-Jones potential coupled with a hard core repulsion. In such cases, the density functional theory (DFT) predicts the formation of several molecular layers near the solid surface where oscillations occur in the fluid density distribution (FDD).[1−4] The consecutive formation of these layers during adsorption generates multiple steps in the adsorption isotherm, which could be predicted by the conventional DFT[3,5,6] and identified experimentally.[7] Experiment also reveals that the steps in the adsorption isotherms are often damped[6] by microscopic heterogeneities present on real surfaces. Several approaches were developed to account for such a heterogeneity (see refs 6 and 8, and references therein). One of the most successful approaches was developed by Neimark et al.,[8] the so-called quenched solid DFT (QSDFT) approach. This approach involves two density distributions: one for the adsorbed fluid and another one for the adsorbent. The latter distribution was assumed to be linear and its two parameters were selected such as to achieve optimum fit with the experimental adsorption isotherms. The density distribution of the fluid component was obtained by minimizing the grand canonical potential of the system with respect to the fluid density. Although QSDFT provides a good description of the experimental results (see ref 8), it involves a phenomenological modeling of the solid density distribution (SDD). Both an intrinsic (in the absence of adsorbate) solid density distribution and an additional deformation caused by the adsorbate occur. They can affect the wetting characteristics of the solid, which are sensitive even to microscopic inhomogeneities of the order of a few angstroms. As examples, one can mention the results obtained in refs 9 and 10, where it was demonstrated theoretically[9] and via molecular dynamics simulation[10] that the presence of asperities with dimensions of only a few angstroms on an ideal hydrophilic surface can considerably increase the contact angle of a nanodrop on such a surface.

In this paper, we outline a procedure which can be used to predict both (the solid and fluid) density distributions, SDD and FDD, on the basis of interaction potentials only. In the present approach, the traditional multicomponent DFT used to describe fluids confined in a pore in contact with an external reservoir of fluid molecules is combined with another one involving a closed system containing a fixed number of molecules that generate the solid. The approach implies that the solid is a continuous medium in which the crystal structure is not taken into account. Such an assumption is frequently used in the literature.[2,11]

2. THE MODEL

The considered system is treated as a mixture of spherical molecules of component A (CA) and component B (CB) confined in a slitlike pore presented schematically in Figure 1. The walls of the slit do not provide external potentials acting on the molecules present inside the slit but serve only as boundaries. One of the components (CB) is connected to a reservoir which contains only molecules of the same component at the chemical potential μ_B. Because the interactions between the molecules of

Received: July 18, 2011
Revised: September 8, 2011
Published: October 10, 2011

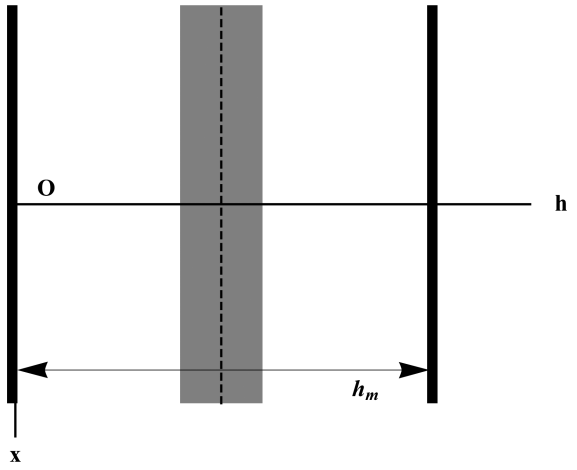

Figure 1. Schematic view of the considered system, consisting of a slit between two neutral, infinite, parallel boundaries separated by the distance h_m and filled with a binary mixture. The shaded rectangle in the middle of the slit represents the solid formed from one of the components. (The density distribution of the solid molecules will be found by solving the appropriate Euler−Lagrange equation considered below.) The vertical dashed line represents the plane of symmetry of the slit. The *y*-axis is normal to the plane of the figure.

CA are assumed to be very strong, it is reasonable to assume that their concentration in the above reservoir is negligible and that the slit contains a fixed number of molecules of CA interacting among themselves and with the molecules of CB. As explained in detail below, the molecules of CA form a solid body (shaded area in Figure 1) with a continuous nonuniform density distribution near the fluid−solid interface.

The interactions between molecules inside the slit are characterized by short-range hard-core repulsions and long-range van der Waals attractions. The latter is calculated using the Weeks−Chandler−Anderson approach[12]

$$U_{ij}(r) = \begin{cases} -\varepsilon_{ij}, & r \le 2^{1/6}\sigma_{ij} \\ 4\varepsilon_{ij}\left[\left(\frac{\sigma_{ij}}{r}\right)^{12} - \left(\frac{\sigma_{ij}}{r}\right)^{6}\right], & r > 2^{1/6}\sigma_{ij} \end{cases} \quad (1)$$

where the subscripts i and j can be A and B corresponding to components A and B, r is the distance between the centers of a pair of interacting molecules, and the constants σ_{ij} and ε_{ij} are hard core diameters and energy parameters, respectively. Because the main purpose of this paper is to provide a procedure able to predict the density distributions of both the solid and fluid, rather than a specific case, the values of the parameters that appear in eq 1 were selected arbitrarily as follows: ε_{BB}/k_B = 119.76 K, σ_{BB} = 3.405 Å, ε_{AA}/k_B = 295.0 K, σ_{AA} = 3.800 Å, ε_{AB}/k_B = 153.0 K, σ_{AB} = 3.530 Å, where k_B is the Boltzmann constant. Note that the parameters for components B and A were selected close to those for argon and solid carbon dioxide, respectively.

The density distributions $\rho_i(\mathbf{r})$ (i = A,B) are calculated using the Rosenfeld et al.[13] version of DFT . The Euler−Lagrange equations for the density distributions $\rho_i(\mathbf{r})$ (i = A,B) have been obtained by minimizing the thermodynamic potential

$$\Omega[\rho_A(\mathbf{r}), \rho_B(\mathbf{r})] = F_{id}[\rho_A(\mathbf{r}), \rho_B(\mathbf{r})] + \Phi[\rho_A(\mathbf{r}), \rho_B(\mathbf{r})] + F_{attr}[\rho_A(\mathbf{r}), \rho_B(\mathbf{r})] - \mu_B \int_V \rho_B(\mathbf{r})\, d\mathbf{r} \quad (2)$$

with respect to the densities $\rho_A(\mathbf{r})$ and $\rho_B(\mathbf{r})$ under the constraint of fixed average density of component A in the slit.

In eq 2, $F_{id}[\rho_A(\mathbf{r}),\rho_B(\mathbf{r})]$ is the Helmholtz free energy of a mixture of ideal gases, $\Phi[\rho_A(\mathbf{r}),\rho_B(\mathbf{r})]$ and $F_{attr}[\rho_A(\mathbf{r}),\rho_B(\mathbf{r})]$ are contributions to the excess free energy due to a system of hard spheres and to the attractive part of intermolecular interactions, respectively. Expressions for these contributions are provided in the Appendix.

The Euler−Lagrange equations for densities $\rho_A(\mathbf{r})$ and $\rho_B(\mathbf{r})$ have the form

$$\log[\Lambda_i^3 \rho_i(\mathbf{r})] - Q_i(\mathbf{r}) = \lambda_i/k_B T, \quad (i = A, B) \quad (3)$$

where the functions $Q_i(\mathbf{r})$ are provided in the Appendix, $\Lambda_i = h_P/(2\pi m_i k_B T)^{1/2}$ is the thermal de Broglie wavelength of the molecules of component i, h_P is the Planck constant, T is the absolute temperature, and m_i is the molecular mass of component i, which were selected as for argon (i = B) and CO_2 (i = A). For component B, $\lambda_B = \mu_B$, where μ_B is the chemical potential in the reservoir. For component A, λ_A is a Lagrange multiplier arising because of the constraint of fixed number of molecules of CA in the slit and determined using this constraint. Equation 3 can be solved using a standard iteration procedure. Due to the uniformity of the system in x and y directions, the densities $\rho_A(\mathbf{r})$ and $\rho_B(\mathbf{r})$ depend only on the distance h from one of the slit walls (see Figure 1).

3. RESULTS AND CONCLUSION

The calculations were carried out at T = 85 K for a slit of width $h_m = 100\sigma_{BB}$ and for an average density of CA in the slit, ρ_A^0, given by $\rho_A^0 {\sigma_{BB}}^3 = 0.2246$. Because the system is symmetric, $\rho_B(h)$ and $\rho_A(h)$ are symmetric with respect to the middle of the slit, $\rho_A(h)$ being located almost completely in a $30\sigma_{BB}$ range around the middle of the slit.

In Figure 2a, the density distributions of CB (dashed lines) and CA (solid lines) are plotted for $\mu_B/k_B T$ = −16.809, −14.1454, and −12.706 corresponding to the bulk pressures P of CB equal to P/P_0 = 0.0058, 0.0835, and 0.288, respectively, where P_0 is the bulk pressure at liquid−vapor coexistence. The density $\rho_A(h)$ of component A increases rapidly over a distance of a few molecular diameters from almost zero to a constant value $\rho_{A,s} = 0.702/{\sigma_{BB}}^3$, where $\rho_{A,s}$ is the bulk density of the solid. Several oscillations are present in the h-dependence of $\rho_A(h)$.

One can define the location h_s of the planar solid surface as the position corresponding to an equimolar dividing surface given by the expression

$$\int_0^{h_m/2} \rho_A(h)\, dh = \rho_{A,s}(h_m/2 - h_s) \quad (4)$$

as illustrated in Figure 2b. (Note that, in addition to the surface located at $h = h_s$, there is also a surface located at $h = h_m - h_s$.) In Figure 2a, the locations h_s of the corresponding surfaces are indicated by dots on each of the solid density profiles. For the profile corresponding to P/P_0 = 0.288 the solid surface is represented by a vertical line.

Figure 2a indicates that the solid surface located via eq 4 is displaced, with increasing bulk pressure, toward the center of the slit, the displacement being of about $0.2\sigma_{BB}$ when P/P_0 varies from 0.0058 to 0.288. Our calculations have shown that the density profile $\rho_A(h)$ remains practically the same for P/P_0 greater than 0.288 and P/P_0 smaller than 0.0058. In the latter case, the solid density profile can be considered as the intrinsic

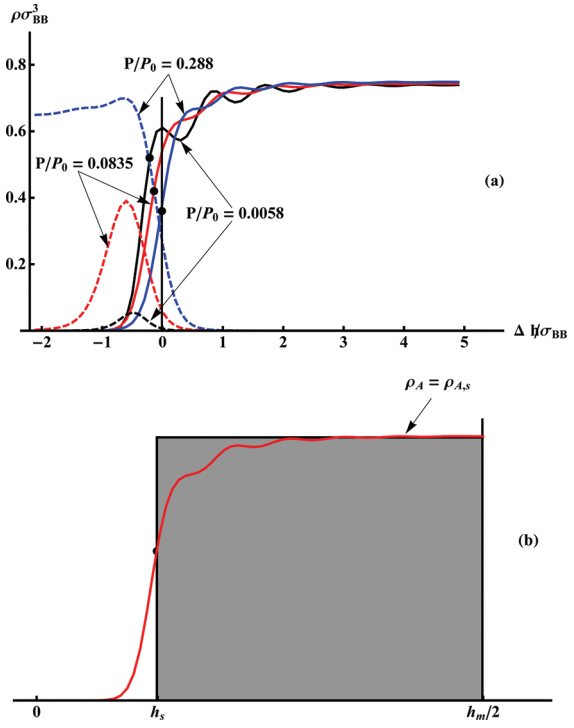

Figure 2. (a) Density distributions of component A (solid lines) and component B (dashed lines) at various bulk pressures P of component B. P_0 is the bulk pressure at the liquid−vapor coexistence. Only a part of the slit on the left-hand side of the plane of symmetry of the slit (see Figure 1) is presented. All densities are represented as functions of the distance $\Delta h = h - h_s^0$, where h_s^0 provides the position of a solid surface calculated using eq 4 for an arbitrarily selected $P/P_0 = 0.288$. (b) Illustration of the location of the planar solid surface at $h = h_s$. h_s is obtained by equating the area of the rectangle to the area under the curve of the actual fluid density distribution (solid line).

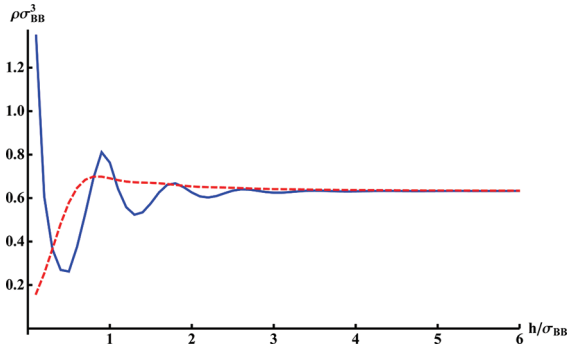

Figure 3. Density profiles of component B near a hard uniform planar wall made of molecules of component A (solid line) as well as near the solid surface considered in the present paper (dashed line).

one, because it is calculated for conditions close to the absence of fluid inside the system. The fluid density profile near a nonhomogeneous solid differs from that near a uniform solid with an ideal planar surface. In Figure 3, density profiles are presented for CB near an ideal uniform planar solid (solid line) and a nonuniform solid (dashed line). The interaction potential between the molecules of the uniform solid and those of CB inside the slit is assumed to be of the Lennard-Jones type coupled with a hard

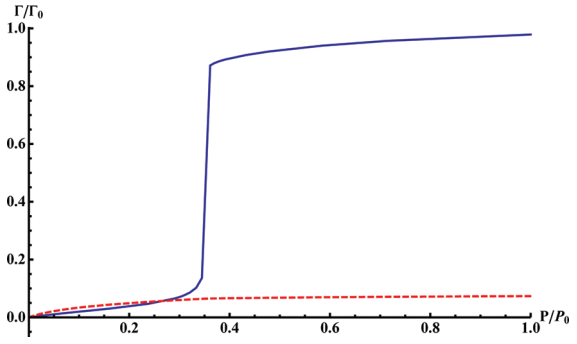

Figure 4. Adsorption isotherm (solid line) in the volume between a slit wall at $h = 0$ and the surface of the nonuniform solid located at $h = h_s$. The dashed line represents the amount of fluid absorbed by the solid multiplied by 50. Γ_0 is the adsorption at the bulk pressure P_0.

core repulsion. The energy and length parameters of the fluid−uniform solid interaction were taken ε_{AB} and σ_{AB}, respectively, and the uniform solid density was assumed to be $\rho_{A,s}$. In this case, the interaction of a fluid molecule with the hard uniform solid is provided by the potential $\psi(h) = (2\pi/3)\varepsilon_{AB}\rho_s\sigma_{AB}^3[(2/15)\cdot((\sigma_{AB})/(\sigma_{AB} + h))^9 - ((\sigma_{AB})/(\sigma_{AB} + h))^3]$.

The main difference between the two fluid density profiles is the absence of oscillations in the vicinity of the nonuniform solid. Such a damping of density oscillations in the fluid density profile also was noted in ref 8, where argon in contact with solid carbon was considered. Such a difference in the behavior of the fluid density profile is expected. Indeed, as well-known, the oscillations of fluid density near the surface of a uniform solid is a consequence of close packing, which leads to the formation of molecular layers near the surface. If the solid is nonhomogeneous, such a layering does not occur because some molecules of CB are absorbed by the solid.

Figure 4 presents an adsorption isotherm of CB (solid curve) calculated for the volume between a slit boundary at $h = 0$ and the surface of the nonuniform solid located at $h = h_s$. The amount of fluid adsorbed per unit area of the solid is provided by equation $\Gamma = \int_0^{h_s}\rho_B(h)\,dh - \rho_{B,bulk}h_s$, where $\rho_{B,bulk}$ is the fluid density in the reservoir. The amount of fluid absorbed by the solid near that surface is presented by the dashed line. As expected, the adsorption isotherm is smooth, free of the multiple steps which were observed near the surface of a uniform solid. The amount of absorbed fluid is small, its fraction compared to that of adsorbed fluid decreasing from 6% at small fluid densities in the reservoir to 0.1% at large densities.

In conclusion, the suggested version of the DFT provides a unified approach for the description of a fluid in contact with a deformable solid surface. Both the fluid and the solid density distributions were obtained from the solution of the appropriate Euler−Lagrange equations. The fluid density profile near a deformable solid does not exhibit the strong oscillations present when the solid is uniform. Another consequence, which was observed experimentally is the absence of steps in the adsorption isotherms. The theory allows to calculate the amount of fluid adsorbed and the amount of fluid absorbed by the solid.

APPENDIX. DERIVATION OF THE EULER−LAGRANGE EQUATION

The density distributions $\rho_i(\mathbf{r})$ $(i = A,B)$ of components A and B are calculated using a modified density functional approach .

The total Helmholtz free energy $F_{tot}[\rho_A(\mathbf{r}),\rho_B(\mathbf{r})]$ is expressed as the sum of an ideal gas free energy, $F_{id}[\rho_A(\mathbf{r}),\rho_B(\mathbf{r})]$, and an excess free energy $F_{ex}[\rho_A(\mathbf{r}),\rho_B(\mathbf{r})]$. The ideal gas free energy contribution has the form

$$F_{id}[\rho_A(\mathbf{r}),\rho_B(\mathbf{r})] = k_B T \sum_{i=A,B} \int d\mathbf{r}\, \rho_i(\mathbf{r})\{\log[\Lambda_i^3 \rho_i(\mathbf{r})] - 1\} \quad (A.1)$$

where $\Lambda_i = h_P/(2\pi m_i k_B T)^{1/2}$ is the thermal de Broglie wavelength of the molecules of component i, k_B and h_P are the Boltzmann and Planck constants,respectively, T is the absolute temperature, and m_i is the molecular mass of component i. The excess free energy contains a contribution from a system of hard spheres $\Phi[\rho_A(\mathbf{r}),\rho_B(\mathbf{r})]$ and a contribution $F_{attr}[\rho_A(\mathbf{r}),\rho_B(\mathbf{r})]$ due to the attractive interactions between molecules. The former contribution has, in Rosenfeld's approximation,[13] the form

$$\Phi[\rho_A(\mathbf{r}),\rho_B(\mathbf{r})]/k_B T = -n_0 \log(1-n_3) + \frac{n_1 n_2 - \mathbf{n}_{1v}\mathbf{n}_{2v}}{1-n_3} + \frac{{n_2}^3 - 3n_2{\xi_0}^2 + 2{\xi_0}^3}{24\pi(1-n_3)^2} \quad (A.2)$$

where n_α (α = 0,1,2,3) and $n_{\alpha v}$ (α = 1,2) are defined as follows

$$n_\alpha(\mathbf{r}) = \sum_{i=A,B} \int d\mathbf{r}'\, \rho_i(\mathbf{r}')\omega_i^{(\alpha)}(\mathbf{r}-\mathbf{r}'), \quad \alpha = 0,1,2,3 \quad (A.3)$$

$$\mathbf{n}_{\alpha v}(\mathbf{r}) = \sum_{i=A,B} \int d\mathbf{r}'\rho_i(\mathbf{r}')\bar{\omega}_i^{(\alpha)}(\mathbf{r}-\mathbf{r}'), \quad \alpha = 1,2 \quad (A.4)$$

and $\xi_0 = ({n_{2v,x}}^2 + {n_{2v,y}}^2 + {n_{2v,h}}^2)^{1/2}$. The scalar, $\omega_i^{(\alpha)}(\mathbf{r}-\mathbf{r}')$, and vector, $\bar{\omega}_i^{(\alpha)}(\mathbf{r}-\mathbf{r}')$, weight functions can be written in the form[14]

$$\omega_i^{(3)}(\mathbf{r}) = \Theta(|\mathbf{r}| - R_i), \quad \omega_i^{(2)}(\mathbf{r}) = \delta(|\mathbf{r}| - R_i) \quad (A.5)$$

$\omega_i^{(1)}(\mathbf{r}) = \omega_i^{(2)}(\mathbf{r})/4\pi R_i$, $\omega_i^{(0)}(\mathbf{r}) = \omega_i^{(2)}(\mathbf{r})/4\pi R_i^2$, $\bar{\omega}_i^{(\alpha)}(\mathbf{r}) = (\mathbf{r}/|\mathbf{r}|)\omega_i^{(\alpha)}(\mathbf{r})$ (α = 1, 2), where R_i is the molecular radius of component i, $\delta(x)$ and $\Theta(x)$ are the δ- Dirac and Heaviside functions, respectively.

The contribution to the excess free energy due to the attraction between the molecules of the mixture, calculated in the mean-field approximation, is given by

$$F_{attr}[\rho_A(\mathbf{r}),\rho_B(\mathbf{r})] = \frac{1}{2}\sum_{i,j=A,B} \int\int d\mathbf{r}\, d\mathbf{r}'\, \rho_i(\mathbf{r})\rho_j(\mathbf{r}')U_{ij}(|\mathbf{r}-\mathbf{r}'|) \quad (A.6)$$

where the interaction potential $U_{ij}(|\mathbf{r}-\mathbf{r}'|)$ is provided by eq 1 in the text of the paper.

The Euler−Lagrange equations for the fluid density distributions $\rho_i(\mathbf{r})$ (i = A,B) can be obtained by minimizing the thermodynamic potential eq 2 with respect to the densities $\rho_A(\mathbf{r})$ and $\rho_B(\mathbf{r})$ of components A and B, respectively, under the constraint of fixed average density of component A in the slit

$$\rho_{A,av} = \frac{1}{V}\int_V d\mathbf{r}\, \rho_A(r) \quad (A.7)$$

where V is the volume of the slit.

These equations have the form of eq 3 where

$$k_B T Q_i(\mathbf{r}) = -\sum_{\alpha=0}^{3}\int d\mathbf{r}'\frac{\partial\Phi}{\partial n_\alpha(\mathbf{r}')}\omega_i^{(\alpha)}(\mathbf{r}-\mathbf{r}') - \sum_{\alpha=1}^{2}\int d\mathbf{r}'\frac{\partial\Phi}{\partial \mathbf{n}_\alpha(\mathbf{r}')}\bar{\omega}_i^{(\alpha)}(\mathbf{r}-\mathbf{r}') - \int d\mathbf{r}'\,[\rho_i(\mathbf{r}')U_{ii}(|\mathbf{r}-\mathbf{r}'|) + \rho_j(\mathbf{r}')U_{ij}(|\mathbf{r}-\mathbf{r}'|)], \quad i,j = A,B(i \neq j) \quad (A.8)$$

For component B, $\lambda_B = \mu_B$ where μ_B is the chemical potential in the reservoir. For component A, λ_A is a Lagrange multiplier arising because of the constraint provided by eq A.7.

Using eqs A.7 and 3, the Lagrange multiplier can be rewritten in the form

$$\lambda_A = -k_B T \log\left[\frac{1}{\rho_{A,av} V {\Lambda_A}^3}\int_V d\mathbf{r}\, e^{Q_A(\mathbf{r})}\right] \quad (A.9)$$

Eliminating λ_A between eqs 3 and A.9 and performing the integration in eq A.8 with respect to the y-direction, one obtains two integral equations for the density distributions $\rho_A(\mathbf{r})$ and $\rho_B(\mathbf{r})$ which can be solved by iterations. Due to the symmetry of the system, the densities $\rho_A(\mathbf{r})$ and $\rho_B(\mathbf{r})$ are functions of the distance h from a slit wall only (see Figure 1). The uniform distributions $\rho_A(h) = \rho_A^0$ and $\rho_B(h) = \rho_B^0$ were selected as initial guesses in the iteration procedure.

AUTHOR INFORMATION

Corresponding Author

*E-mail: feaeliru@buffalo.edu. Phone: (716)645-1179. Fax: (716)645-3822.

REFERENCES

(1) Tarazona, P.; Marconi, U. M. B.; Evans, R. *Mol. Phys.* **1987**, *60*, 573–595.
(2) Evans, R. *J. Phys.: Condens. Matter* **1990**, *2*, 8989–9007.
(3) Lastoskie, C.; Gubbins, K. E.; Quirke, N. *Langmuir* **1993**, *9*, 2693–2702.
(4) Neimark, A. V.; Ravikovitch, P. I.; Vishnyakov, A. *J. Phys.: Condens. Matter* **2003**, *15*, 347–365.
(5) Ravikovitch, P. I.; Vishnyakov, A.; Russo, R.; Neimark, A. V. *Langmuir* **2000**, *16*, 2311–2320.
(6) Ravikovitch, P. I.; Vishnyakov, A.; Neimark, A. V. *Phys. Rev. E* **2001**, *64*, 011602.
(7) Larher, Y.; Angerand, F.; Maurice, Y. *J. Chem. Soc., Faraday Trans. 1* **1987**, *83*, 3355–3366.
(8) Neimark, A. V.; Lin, Y. Z.; Ravikovitch, P. I.; Thommes, M. *Carbon* **2009**, *47*, 1617–1628.
(9) Berim, G. O.; Ruckenstein, E. *J. Colloid Interface Sci.* **2011**, *359*, 304–310.
(10) Daub, C. D.; Wang, J. H.; Kudesia, S.; Bratko, D.; Luzar, A. *Faraday Discuss.* **2010**, *146*, 67–77.
(11) Ebner, C.; Saam, W. F. *Phys. Rev. Lett.* **1977**, *38*, 1486–1489. Szybisz, L.; Sartarelli, S. A. J. *Chem. Phys.* **2008**, *128*, 124702.
(12) Weeks, J. D.; Chandler, D.; Andersen, H. C. *J. Chem. Phys.* **1971**, *54*, 5237–5247.
(13) Rosenfeld, Y.; Schmidt, M.; Lowen, H.; Tarazona, P. *Phys. Rev. E* **1997**, *55*, 4245–4263.
(14) Roth, R.; Dietrich, S. *Phys. Rev. E* **2000**, *62*, 6926–6936.